Beating Ringdowns of Near-Degenerate Mechanical Resonances

Matthijs H.J. de Jong,[1,2] Andrea Cupertino,[1] Dongil Shin,[1,3] Simon Gröblacher,[2] Farbod Alijani,[1] Peter G. Steeneken,[1,2] and Richard A. Norte[1,2,*]

[1] *Department of Precision and Microsystems Engineering, Delft University of Technology, Mekelweg 2, 2628 CD Delft, Netherlands*

[2] *Department of Quantum Nanoscience, Kavli Institute of Nanoscience, Delft University of Technology, Lorentzweg 1, 2628 CJ Delft, Netherlands*

[3] *Department of Materials Science and Engineering, Delft University of Technology, Mekelweg 2, 2628 CD Delft, Netherlands*

(Received 16 November 2022; revised 10 April 2023; accepted 31 July 2023; published 22 August 2023)

Mechanical resonators that possess coupled modes with harmonic frequency relations have recently sparked interest due to their suitability for controllable energy transfer and non-Hermitian dynamics. Here we show coupling between high-Q-factor (greater than 10^4) resonances with a nearly 1:1 frequency relation in spatially symmetric microresonators. We develop and demonstrate a method to analyze their dynamical behavior based on the simultaneous and resonant detection of both spectral peaks, and validate this with experimental results. The frequency difference between the peaks modulates their ringdown, and creates a beat pattern in the linear decay. This method applies to both the externally driven regime and the Brownian-motion (thermal) regime, and allows characterization of both linear and nonlinear parameters. The mechanism behind this method renders it broadly applicable to both optical and electrical readout, as well as to different mechanical systems. This will aid studies using near-degenerate mechanical modes, for example, optomechanical energy transfer, synchronization, and gyroscopic sensors.

DOI: 10.1103/PhysRevApplied.20.024053

I. INTRODUCTION

The dynamics of coupled resonators have been intensely studied from numerous perspectives over the last few centuries. With the advent of ultrahigh-Q mechanical resonators (see Refs. [1–4] as recent examples), the regime of linear coupling between resonances [5–7] has seen renewed interest, due to the sensitivity to small perturbations. High-Q resonators can be used for their long coherence times and lifetimes [8–10], but they often feature spatial symmetries that naturally predispose them to have (near-)degenerate or harmonically related eigenmodes (e.g., Refs. [11–14]). In the case of trampoline membranes, the near-degenerate eigenmodes make them ideal candidates for various schemes in optomechanics, such as synchronization and phonon lasing [15–19], or heat and energy transport [20–22]. Other effects, such as mechanical squeezing [23–26] and noise cancellation [27–30] have been shown in a variety of geometries. Mechanical systems with near-degenerate eigenmodes are an attractive platform for studying exceptional points, nonreciprocal coupling, and other phenomena of non-Hermitian (open) systems [31–35]. An exceptional point, for example, requires the frequencies of the eigenmode to be degenerate and the decay rates to be opposite (e.g., one mode is driven and the other mode decays). Additionally, near-degenerate mechanical resonances have direct applications to sensors such as gyroscopes [36,37].

Because of the development of suspended microscale and nanoscale resonators, some recent studies have focused on the nonlinear behavior of coupled mechanical modes. Coupled nonlinear modes [38–40] can lead to stabilization [41] and low-noise oscillators. Strong coupling [42] can be used in mechanical signal processing, while coherent decay paths [43,44] and nonlinear decay paths [45–47] could be leveraged for controlling energy transfer between modes [48].

In this work, we leverage our fabrication precision to design and study high-Q-factor mechanical modes with a 1:1 frequency relation. On the basis of structures with spatial symmetries and modeling by finite-element methods, we find pairs of modes whose shapes are identical except for a rotation by 90° in the plane of the suspended structures. Measurements of these modes show two peaks in the displacement spectrum that are separated in frequency by less than six parts per million. The energy decay shows two different decay rates, which we can extract without resolving the two spectral peaks. There is evidence that energy

*r.a.norte@tudelft.nl

is exchanged between these two resonances, which indicates a coupling mechanism. We distinguish between the frequency splitting of the peaks due to fabrication imperfections and the frequency splitting due to this coupling using a characterization method based on the simultaneous, resonant detection of both peaks. The detector has a bandwidth larger than the total frequency difference, such that we measure the superposition of both peaks. On the basis of the frequency difference and relative amplitudes of the peaks, we observe a characteristic beat pattern by performing ringdown measurements. From these ringdown measurements, we can extract damping rates γ_1 and γ_2 of the seemingly uncoupled peaks (i.e., decay follows the expected exponential trend). Because of the difference between the peak frequencies ω_1 and ω_2, a characteristic beat pattern appears, with an amplitude inversely proportional to the relative amplitude difference between the two spectral peaks. Modeling of this effect provides evidence of a small coupling between the two (unhybridized) modes with rate J and of a frequency shift due to a small Duffing nonlinearity, and it allows us to investigate the resonator phase decoherence in the thermal-motion (Brownian-motion) regime.

II. RESULTS

A. Coupling and beating

We study the dynamics of near-degenerate mechanical modes using optical interferometers, shown schematically in Fig. 1(a). Two types of resonator are studied: trampoline membranes [1] and spiderweb resonators [3]. A free-space readout system is used for trampoline membranes [Fig. 1(a), left], while the narrow beams of the spiderwebs necessitate a lensed-fiber readout [Fig. 1(a), right]. Application of a resonant drive to a piezoelectric shaker mounted on the sample holder excites mechanical modes of the resonator. By stopping the drive and letting the amplitude decay, we perform a ringdown experiment that allows precise measurement of the decay rate.

The amplitude of a linear harmonic oscillator decays exponentially, which we observe in the motion of the fundamental and third modes of the trampoline membranes [Fig. 1(b), purple and brown lines]. These fit well to a straight line (black) when plotted on a logarithmic scale. The ringdown trace at 240 kHz shows significantly different behavior, corresponding to two different slopes, i.e., two different decay rates. The extracted Q factors (red and orange lines indicate fits) differ by almost an order of magnitude. We show that this peculiar ringdown behavior is due to the near degeneracy of two membrane modes [simulated shapes are shown in the insets in Fig. 1(b)]. This near degeneracy is present for the second mode of the membranes due to symmetry, but is absent for the fundamental and third modes. In the following, we refer to the two near-degenerate (second) modes as peaks with indices 1 and 2.

To model the ringdown with near degeneracy, we start with two (unhybridized) modes, $X_1 = \phi_1(\vec{r})x_1(t)$ and $X_2 = \phi_2(\vec{r})x_2(t)$, where mode shapes $\phi_1(\vec{r})$ and $\phi_2(\vec{r})$ describe the spatial form of the mode through position vector $\vec{r}$, and generalized coordinates $x_1(t)$ and $x_2(t)$ describe the oscillating behavior in time. We obtain the mode shapes from finite-element simulations of our structure, and on the basis of the symmetry of the structure and similarity of the two mode shapes, the effective masses of the unhybridized modes should be equal. We add to our model the decay rates γ_1 and γ_2, the resonance frequencies ω_1 and ω_2, and a linear coupling with rate J [5]. This coupling leads to hybridization, such that the eigenmodes of the system of equations are formed by linear superpositions of x_1 and x_2. This coupling J could, for instance, occur via the substrate to which the resonator is anchored [49–51]. In a ringdown measurement, we observe only the decay, so our model does not need driving terms or noise sources; the initial amplitudes $x_1(t=0)$ and $x_2(t=0)$ of both unhybridized modes are nonzero. Thus we obtain the following set of equations of motion:

$$\begin{aligned} \ddot{x}_1 + \gamma_1\dot{x}_1 + \omega_1^2 x_1 + J^2 x_2 &= 0, \\ \ddot{x}_2 + \gamma_2\dot{x}_2 + \omega_2^2 x_2 + J^2 x_1 &= 0. \end{aligned} \tag{1}$$

It bears mention that the system in Eq. (1) can always be diagonalized to obtain the eigenmodes with coordinates y_1 and y_2 and frequencies ω_1' and ω_2', which are decoupled (see also Supplemental Material [52], Sec. A). Both descriptions yield the same dynamics if their parameters are properly matched. We do not diagonalize Eq. (1) but we keep coordinates x_1 and x_2. This allows us to distinguish between the frequency difference $\omega_2 - \omega_1$ that comes from fabrication imperfections and the frequency difference due to coupling J. This is required to separate the two contributions to the beating effect of Eq. (2), one from energy transfer and the other from the frequency difference. Furthermore, using the amplitudes of the unhybridized modes x_1 and x_2 allows us to add a difference in detection efficiency to x_1 and x_2 based on the mode shapes and the position where the displacement is measured. Finally, we work in the weakly coupled regime, so x_1 and x_2 are not too different from y_1 and y_2.

The spectrum of our resonator at around 240 kHz shows two distinct peaks separated by 9 Hz, as schematically shown in Fig. 1(c) (see also Supplemental Material [52], Sec. B). They can be distinguished and fitted with a sum of two Lorentzians without overlap of the confidence interval of the center frequency, so we refer to them as "near degenerate." However, this frequency difference is smaller than the detection bandwidth of our spectrum analyzer during

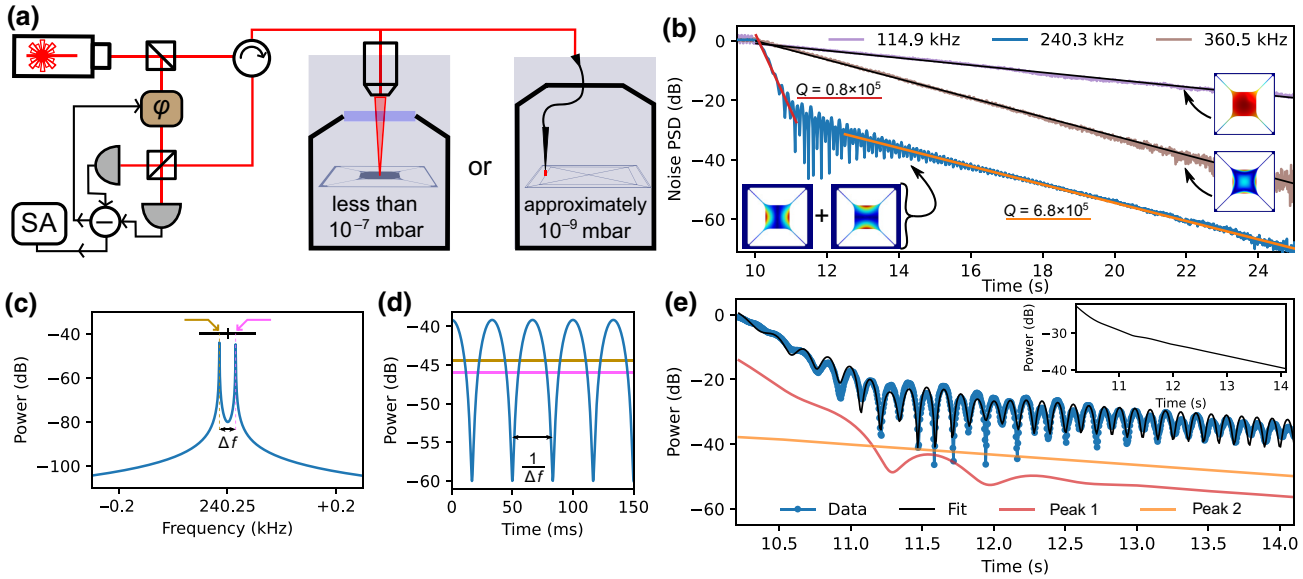

FIG. 1. (a) The two homodyne-detection setups used to measure the mechanical motion of membranes (left) or spiderwebs (right). The sketched laser positions match experimental conditions. (b) Ringdowns of the first three membrane modes (the insets show the mode shape; red indicates maximum displacement). They are aligned to the time where the driving is stopped, at $t = 10$ s. The fundamental (purple) and third (brown) modes can be fitted with single linear slopes (black), while the second mode shows two distinctly different linear slopes (red and orange, with fitted Q factors) and a characteristic beat pattern. The spectrum measured at around this frequency shows two near-degenerate peaks that we associate with the symmetric (simulated) mode shapes indicated in the inset. (c) Simulated spectrum of two modes that exist as distinct spectral peaks separated by less than the detection bandwidth (black bar). (d) The frequency difference Δf leads to a characteristic beat in the ringdown signal. The relative amplitudes of the modes (horizontal gold and pink lines) determine the amplitude of the beat pattern. (e) Simulated amplitudes of near-degenerate peaks 1 and 2 based on extracted decay rates from (b), reconstructed signal with the beat pattern (black), and the measured data (blue). Amplitudes are vertically offset for clarity. The inset shows the total power in the simulation, ignoring the detection efficiency. This is to verify that the energy monotonically decreases, as expected from a system with decay. PSD, power spectral density; SA, spectrum analyzer; ϕ, phase shifter.

the ringdown measurement, such that both peaks are captured in the single ringdown trace. This condition explains the observation of two different slopes in the same ringdown measurement, as the two modes we observe have different decay rates. The slopes are each fitted to a single-exponential decay. The mode with the fastest decay rate is (typically) more susceptible to the drive, such that its amplitude dominates the signal at the start of the ringdown measurement. For short timescales, we thus observe mainly the fast-decaying mode. At longer timescales, the slowly decaying mode dominates the signal, as the fast-decaying mode has lost most of its amplitude. This means that for long timescales, we observe mainly the slowly decaying mode. This leads to a single ringdown measurement showing two different slopes, and allows us to extract the decay rates of the two modes without spectrally resolving them.

The difference in the Q factor between the near-degenerate modes appears similar to the spread in the Q factors of fundamental modes of nominally identical devices (see, e.g., Refs. [51,53]). This spread is commonly attributed to local fabrication imperfections or material variations. Optical-microscope images cannot always corroborate these explanations, since local material impurities (C, O, etc.) are too small to resolve optically. Both fabrication imperfections and material variations are local, and the two near-degenerate modes exist in the same device. However, the deflection profile is different, so the modes can be affected differently. In this way, these effects could cause the difference in the Q factor between near-degenerate modes.

In the kink between the two slopes (red and orange), we observe a particular beat pattern. Such patterns commonly indicate energy exchange [5,6]. However, the coupling rate necessary to create a beat pattern with the frequency we observe would mean that we are in the strong-coupling regime. This regime is incompatible with the observation of the two (different) slopes, since strong coupling allows the energy to decay via the fastest-decaying mode, i.e., one would see only the steepest slope (see Supplemental Material [52], Sec. C). Furthermore, the observed beat pattern is particular because it starts small in amplitude [at

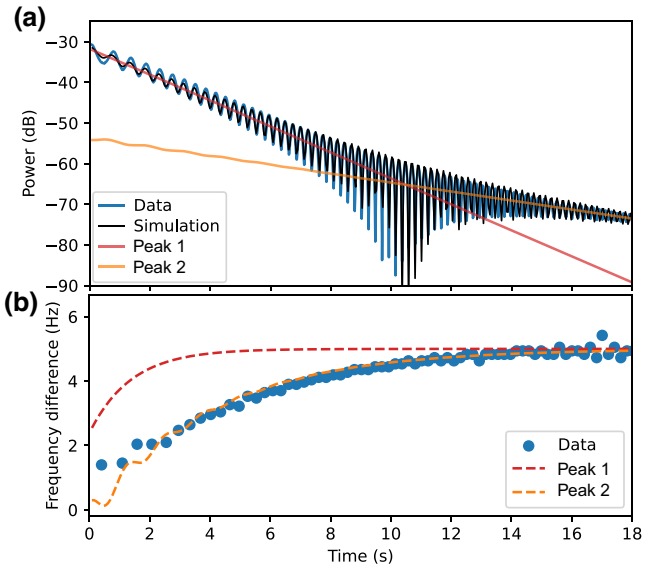

FIG. 2. (a) Ringdown with a prominent beat pattern, measured (blue) and simulated (red, orange, and black). This experiment is performed on a device different from the devices in Fig. 1, but in the same experimental setup. Two separate, linear slopes can be distinguished, but they are similar since the decay rates of both peaks are similar. (b) Frequency difference between the two near-degenerate peaks as the ringdown progresses, determined from the distance between subsequent minima in (a). The fit (orange) is an exponential described in the main text.

$t = 0$ s in Fig. 2(a)], grows until some point ($t = 10.5$ s), but then decreases in amplitude again ($t = 18$ s). Beat patterns in ringdowns due to energy exchange typically show a decrease in amplitude only of the beat pattern [46,47].

Instead, we propose a different effect that contributes to the beat pattern. The signal measured in a ringdown measurement is the total displacement of the resonator, which is the sum of the displacement of both coordinates x_1 and x_2 at the detection spot [Fig. 1(a)]. The total detected displacement power is thus of the form

$$x^2 = |e^{i\omega_1 t}\bar{x}_1 + e^{i\omega_2 t} d\bar{x}_2|^2, \tag{2}$$

where we have split the coordinates x_1 and x_2 into envelopes $\bar{x}_1$ and $\bar{x}_2$ and fast-oscillating terms $e^{i\omega_1 t}$ and $e^{i\omega_2 t}$. The bandwidth of our detector (100 Hz) makes it much slower than the frequencies ω_1 and ω_2 (approximately 240 kHz). We have assumed equal effective masses in Eq. (1), but in principle the effective masses are dependent on the position where the displacement is measured and the shape of the mode [61]. To ensure energy conservation when matching our model with experimental observations, we must introduce a relative detection efficiency d. This constant factor is a function of the position where we measure the resonator displacement and the two simulated mode shapes.

The frequency difference $\Delta f = \omega_2 - \omega_1$ [gold and pink in Figs. 1(c) and 1(d)] creates a beat with period $1/\Delta f$, which is slow enough to be detected. This means the detected displacement power x^2 gains a periodic modulation, a beating that is proportional only to the frequency difference between the peaks and that does not imply energy transfer between them. This effect is well understood as a beat between signals (see, e.g., Ref. [40]), and it applies to different detection mechanisms (optical and electrical) since it requires only the bandwidth of the resonant detector to encompass both peaks. It is analogous to electronically or optically down-mixing a signal by sending in a different tone and observing the beat pattern. In this instance, it is passively obtained on the basis of the small frequency difference between the peaks and the high Q factor of the resonances involved.

To correctly fit the measured ringdown [Fig. 1(e)], we require both the linear coupling and the beating effect. Without the latter, the frequency of the beat pattern would indicate strong coupling, but this is incompatible with the presence of two slopes [5]. Without the former, the beat pattern would appear only briefly in the ringdown as the peak amplitudes cross (see Supplemental Material [52], Sec. C), whereas it extends much further in Fig. 1(e). A nonlinear coupling (proportional to x^3) would lead to a beat pattern that is qualitatively different from the one observed: the beating would slow down in frequency as the amplitude decays (see Supplemental Material [52] Sec. C for a comparison of the linear and nonlinear models).

We obtain the individual center frequencies $\omega_1 = 2\pi \times (240\,331.6 \pm 0.1)$ Hz and $\omega_2 = 2\pi \times (240\,341.4 \pm 0.1)$ Hz of the peaks from a separate spectrum measurement (see Supplemental Material [52], Sec. B) that also allows us to estimate the detection efficiencies [$d \simeq 20$ in Fig. 1(e)]. From the linear parts of the ringdown, we extract decay rates $\gamma_1 = 2\pi \times (6.0 \pm 0.1)$ Hz and $\gamma_2 = 2\pi \times (0.707 \pm 0.001)$ Hz. We can simulate the ringdown using only three fit parameters: the initial positions x_{10} and x_{20} and coupling rate J. The optimized fit (black) to the data (blue) is shown in Fig. 1(e), with dimensionless initial positions $x_{10} = 0.089 \pm 0.001$ and $x_{20} = 0.071 \pm 0.001$ and coupling $J/2\pi = 320 \pm 5$ Hz. The frequency shift due to the linear coupling, J^2/ω_1, would correspond to 0.4 Hz if $\omega_1 = \omega_2$, so we are in the weakly coupled regime. Nonetheless, there is sufficient coupling to observe energy exchange between the reconstructed powers of the unhybridized modes [red and orange lines in Fig. 1(e)]. For example, between 11.3 s and 11.5 s, x_1 gains energy from x_2, shown by the increase of the reconstructed power. The power in x_2 correspondingly decreases, but this is not clearly visible in Fig. 1(e) due to the difference in detection efficiency. We numerically verify that the reconstructed power always decreases over time, as shown by plotting the total power in the inset in Fig. 1(e). Our measurement thus marks the observation of purely linear coupling

between two resonances with a near-degenerate frequency relation, without showing nonlinear power decay.

B. Frequency shift

The beat pattern is periodic with the inverse of the frequency difference between the two near-degenerate peaks. Careful study of Fig. 1(e) shows that this period is not constant; it changes with time. This means that the frequency difference is not constant, and that either one peak or both peaks change in frequency over time, similarly to what was reported in Ref. [40]. In the previous section, the energy decay was observed to be linear, sufficiently so that no nonlinearity is necessary to describe the ringdown completely. However, a small nonlinearity might still be present and lead to a frequency shift without measurably affecting the energy decay. Since the period of the beating is inversely proportional to the frequency difference, analysis of this periodicity provides a measure sensitive to small nonlinearities.

From the ringdown shown in Fig. 2(a), we extract the frequency difference by finding the minima of the beat pattern and taking the inverse of their time differences. We plot the frequency difference in Fig. 2(b) (blue), which shows an exponential trend towards $\Delta f = 5.0$ Hz. It is likely that the drive pulled the frequencies of the two peaks together [54], which indicates the presence of a nonlinearity. Assuming a small Duffing nonlinear term (proportional to x^3), the frequency shift due to frequency pulling is of the form [54]

$$\omega_{\mathrm{NL}} = \omega_0 + \frac{3}{8}\frac{\alpha}{m_{\mathrm{eff}}\omega_0}\tilde{x}^2, \tag{3}$$

with Duffing coefficient α, effective mass m_{eff}, and displacement amplitude $\tilde{x}$.

By observing the change in the frequency difference, we can extract which of the two peaks behaves nonlinearly, and whether it is softening or hardening. The linear parameters are extracted by the same procedure as before (the frequencies follow from a spectrum measurement, and the decay rates are fits to the linear parts of the ringdown and their coupling is modeled via Eq. 1). We find $\omega_1 = 2\pi \times (240\,302.4 \pm 0.2)$ Hz, $\gamma_1 = 2\pi \times (0.71 \pm 0.01)$ Hz, $\omega_2 = 2\pi \times (240\,307.4 \pm 0.1)$ Hz, $\gamma_2 = 2\pi \times (0.218 \pm 0.001)$ Hz, and $J = 2\pi \times (20 \pm 1)$ Hz (independent of the value of α) with relative detection efficiency $d \simeq 50$. We calculate the frequency shift as the peak amplitude decays from Eq. (3). The decay rates are different, which means that their frequency shift should change over time at different rates, as illustrated by the dashed lines in Fig. 2(b). The measured frequency shift is consistent with peak 2 being frequency-pulled by the drive. This implies a softening nonlinearity ($\alpha < 0$), which is usually associated with an external (e.g., electrical or optical) force source (geometric nonlinearity tends to yield hardening behavior [40,55]). However, curvature of the membrane in the out-of-plane direction could also lead to a softening nonlinearity. Although the suspended membrane is nominally flat due to the tensile stress, some curving at the membrane edges can be observed under a microscope (see, the supplementary information for Ref. [56]). In the absence of any external sources of (softening) nonlinearity, this curvature could be responsible for the observed change in the periodicity of the beat pattern. Buckling [57] of the whole membrane is unlikely given the high fabrication prestress (1 GPa). An estimate for α based on the onset of the Brownian-motion regime yields $\alpha_2 = -3 \times 10^{-21}$ m^{-2} s^{-2}, but a more-accurate value should be obtained after calibration of the displacement and detection efficiency. The nonlinear term is sufficiently small compared with the coupling J that it is negligible for the measured ringdowns. Despite this, we can observe and measure the frequency shift due to the nonlinearity. Comparison with the literature shows that our method is 3 orders of magnitude more sensitive than the method reported in Ref. [40], which uses a similar technique but for GaAs nanowires.

C. Resonator decoherence

Frequency shifts of resonators due to external factors are associated with resonator phase decoherence [9] or dephasing. This is detrimental for coherent control [8,10], which is important for many quantum mechanical applications. Classically, one can observe the spectral width integrated over sufficient time to obtain the phase decoherence time [9]. We describe how the beating effect provides another mechanism to evaluate the phase decoherence time by utilizing the second peak as a frequency reference.

In spiderweb resonators [3], there is a set of modes extremely close to degeneracy, which we observe as two peaks at frequencies $\omega_1 = 2\pi \times (120\,725.517 \pm 0.002)$ Hz and $\omega_2 = 2\pi \times (120\,726.141 \pm 0.001)$ Hz (a difference of less than six parts per million), as shown in Figs. 1(a) and 3(a). These peaks have linewidths below the resolution of the spectrum analyzer in this setup (0.01 Hz). We estimate their spectral linewidths to be 2.5 and 2.3 mHz, respectively (full width at half maximum, corresponding to $Q \simeq 25 \times 10^6$), which matches the Q factor extracted from a linear fit to the ringdown measurement: $Q = 21.1 \times 10^6$.

The ringdown measurement [Fig. 3(b)] shows the beat pattern both in the strongly driven regime (blue) and in the Brownian-motion regime (green). The dynamics of x_1 and x_2 are much faster than our detection bandwidth, and we work at room temperature, so we cannot directly resolve the thermal decoherence rate [10]. However, the beat pattern is sensitive to frequency fluctuations. A phase shift in the beat pattern corresponds to a frequency shift between the two peaks. Thus, monitoring the beat-pattern phase

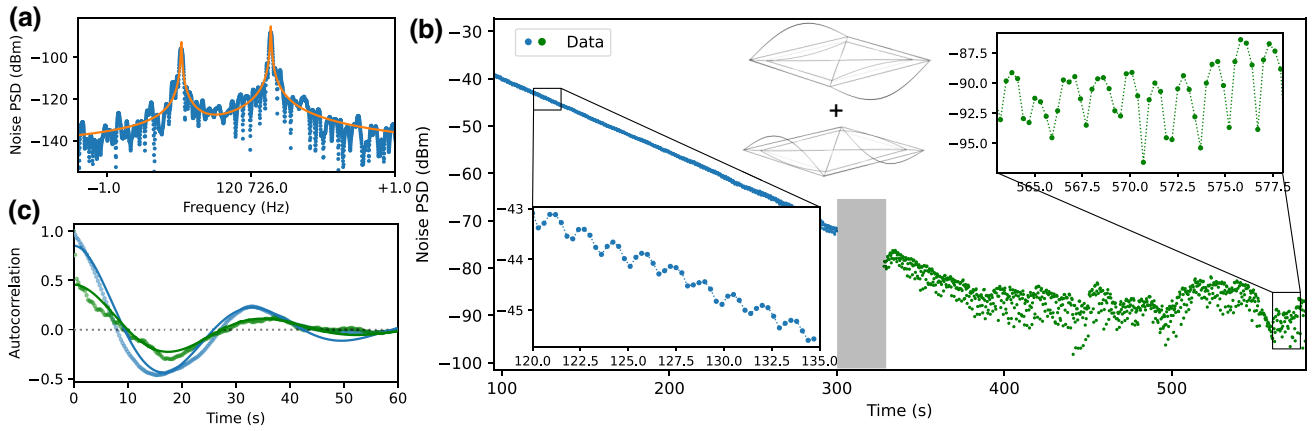

FIG. 3. (a) Mechanical spectrum of near-degenerate modes of a spiderweb resonator (blue), with Lorentzian fits (orange). (b) Two consecutive ringdowns performed on the same device, one showing the decay from the driven state (blue) and the other showing the last part of the ringdown and subsequent transition towards a Brownian-motion-driven state (green). The insets highlight the beating behavior (dotted line drawn as a guide for the eye), which continues even in the Brownian-motion regime. The gray region denotes the cut between the two ringdowns. The two simulated mode shapes are shown schematically. (c) Autocorrelation functions of the signal in the ringdown (blue) and Brownian-motion regime (green), showing a coherence time of 24 ± 2 s. Points indicate the experimental data and solid lines indicate the fit. PSD, power spectral density.

allows us to observe frequency shifts, which correspond to phase decoherence between the two observed modes. We can do so by calculating the autocorrelation of the beating signal in Fig. 3(b), which we plot in Fig. 3(c). It shows behavior similar to that of a single, underdamped particle on a spring undergoing Brownian motion, which has an autocorrelation given by [58]

$$C(t) = \frac{\Gamma k_B T}{m_{\text{eff}}} e^{-\Gamma t} \left(\frac{1}{\Gamma} \cos(\delta t) - \frac{1}{\delta} \sin(\delta t) \right), \qquad (4)$$

with $\delta = \sqrt{\Omega^2 - \Gamma^2}$. Here the frequency Ω is the frequency of the beat pattern, and the decay Γ is related to the phase decoherence time, i.e., when the amplitude of the autocorrelation drops by half. We fit $1/\Gamma = 24.5 \pm 1.8$ s ($1/\Gamma = 24.8 \pm 2.8$ s) in the driven (thermal) regime. This is close to the linear (energy) decay time ($Q/\omega_1 = Q/\omega_2 \simeq 27.8$ s) extracted from the ringdown directly. This is the expected behavior for a linear harmonic oscillator: the phase decoherence time (measured via the beat pattern) should be similar to the energy decay time (measured directly from the ringdown). Additionally, we fit $\Omega = 0.195 \pm 0.001$ Hz ($\Omega = 0.185 \pm 0.002$ Hz) in the driven (thermal) regime, which matches well with the frequency difference between the two peaks $|\omega_1 - \omega_2|/\pi$. This illustrates that the beating effect can provide a measurement of the phase decoherence of (near-)degenerate modes of a mechanical resonator.

III. CONCLUSION

We have experimentally studied high-Q-factor mechanical modes of spatially symmetric microresonators that are near degenerate. We provide evidence of a linear coupling between the two resonances, present without driving the resonator to nonlinearity. This is in contrast to previous studies, which generally required a quadratic or cubic term for coupling. To detect this linear coupling, we developed a characterization method based on a single, resonant detector. This detector has a detection bandwidth that encompasses both spectral peaks, such that we can see two decay rates in a single ringdown measurement. When the spectral peaks are sufficiently close in frequency, an interference effect occurs that leads to a particular beat pattern. The relative amplitudes of the individual peaks control the beat-pattern amplitude, while their frequency difference controls the beating period. From the beat pattern, we can monitor the amplitudes of the individual spectral peaks and find their coupling rate. The beating period provides a sensitive measure to the relative frequency difference between the two peaks. This allows us to observe slight frequency shifts due to nonlinearities, which would be difficult to observe with other methods. Our Si_3N_4 trampoline membranes feature a softening nonlinearity, which we attribute to out-of-plane curving. The beating period can additionally be used to monitor frequency shifts associated with phase decoherence of the modes. In Si_3N_4 spiderweb resonators, we find the phase decoherence time is similar to the energy decay time, as expected for linear harmonic oscillators.

Our characterization method is applicable to both optical and electrical readout schemes, and is particularly suited to high-Q-factor mechanical resonators. This type of resonator is highly relevant for, for example, sensing and optomechanics and forms an attractive platform to study non-Hermitian systems. We have thus developed a broadly applicable method to characterize near-degenerate resonators, which can be immediately applied to studies in different fields.

All data, simulations, and measurement and analysis scripts in this work are available at [62].

ACKNOWLEDGMENTS

R.N. acknowledges support from the Limitless Space Institute's I2 Grant. This publication is part of the project "Probing the physics of exotic superconductors with microchip Casimir experiments" (740.018.020) of the NWO START-UP research program, which was partly financed by the Dutch Research Council (NWO). M.H.J.d.J., A.C., and R.A.N. acknowledge valuable support from Kavli Nanolab Delft and from the technical support staff of the Department of Precision and Microsystems Engineering of the Faculty of Mechanical, Maritime and Materials Engineering of Delft University of Technology.

[1] R. A. Norte, J. P. Moura, and S. Gröblacher, Mechanical Resonators for Quantum Optomechanics Experiments at Room Temperature, Phys. Rev. Lett. **116**, 147202 (2016).

[2] Y. Tsaturyan, A. Barg, E. S. Polzik, and A. Schliesser, Ultracoherent nanomechanical resonators via soft clamping and dissipation dilution, Nat. Nanotechnol. **12**, 776 (2017).

[3] D. Shin, A. Cupertino, M. H. J. de Jong, P. G. Steeneken, M. A. Bessa, and R. A. Norte, Spiderweb nanomechanical resonators via Bayesian optimization: Inspired by nature and guided by machine learning, Adv. Mater. **34**, 2106248 (2022).

[4] M. J. Bereyhi, A. Arabmoheghi, S. A. Fedorov, A. Beccari, G. Huang, T. J. Kippenberg, and N. J. Engelsen, Perimeter Modes of Nanomechanical Resonators Exhibit Quality Factors Exceeding 10^9 at Room Temperature, Phys. Rev. X **12**, 021036 (2022).

[5] D. H. Zanette, Energy exchange between coupled mechanical oscillators: linearregimes, J. Phys. Commun. **2**, 095015 (2018).

[6] S. R.-K. Rodriguez, Classical and quantum distinctions between weak and strong coupling, Eur. J. Phys. **37**, 025802 (2016).

[7] G. Dolfo and J. Vigué, Damping of coupled harmonic oscillators, Eur. J. Phys. **39**, 025005 (2018).

[8] T. Faust, J. Rieger, M. J. Seitner, J. P. Kotthaus, and E. M. Weig, Coherent control of a classical nanomechanical two-level system, Nat. Phys. **9**, 485 (2013).

[9] B. H. Schneider, V. Singh, W. J. Venstra, H. B. Meerwaldt, and G. A. Steele, Observation of decoherence in a carbon nanotube mechanical resonator, Nat. Commun. **5**, 5819 (2014).

[10] D. J. Wilson, V. Sudhir, N. Piro, R. Schilling, A. Ghadimi, and T. J. Kippenberg, Measurement-based control of a mechanical oscillator at its thermal decoherence rate, Nature **524**, 325 (2015).

[11] A. Gloppe, P. Verlot, E. Dupont-Ferrier, A. Siria, P. Poncharal, G. Bachelier, P. Vincent, and O. Arcizet, Bidimensional nano-optomechanics and topological backaction in a non-conservative radiation force field, Nat. Nanotechnol. **9**, 920 (2014).

[12] L. Mercier de Lépinay, B. Pigeau, B. Besga, and O. Arcizet, Eigenmode orthogonality breaking and anomalous dynamics in multimode nano-optomechanical systems under nonreciprocal coupling, Nat. Commun. **9**, 1401 (2018).

[13] D. Hälg, T. Gisler, E. C. Langman, S. Misra, O. Zilberberg, A. Schliesser, C. Degen, and A. Eichler, Strong Parametric Coupling between Two Ultra-coherent Membrane Modes, Phys. Rev. Lett. **128**, 094301 (2022).

[14] G. La Gala, J. P. Mathew, P. Neveu, and E. Verhagen, Nanomechanical design strategy for single-mode optomechanical measurement, J. Phys. D: Appl. Phys. **55**, 225101 (2022).

[15] G. Heinrich, M. Ludwig, J. Qian, B. Kubala, and F. Marquardt, Collective Dynamics in Optomechanical Arrays, Phys. Rev. Lett. **107**, 043603 (2011).

[16] C.-G. Liao, R.-X. Chen, H. Xie, M.-Y. He, and X.-M. Lin, Quantum synchronization and correlations of two mechanical resonators in a dissipative optomechanical system, Phys. Rev. A **99**, 033818 (2019).

[17] M. Zhang, G. S. Wiederhecker, S. Manipatruni, A. Barnard, P. McEuen, and M. Lipson, Synchronization of Micromechanical Oscillators Using Light, Phys. Rev. Lett. **109**, 233906 (2012).

[18] J. Sheng, X. Wei, C. Yang, and H. Wu, Self-Organized Synchronization of Phonon Lasers, Phys. Rev. Lett. **124**, 053604 (2020).

[19] Q. Zhang, C. Yang, J. Sheng, and H. Wu, Dissipative coupling induced phonon lasing with anti-parity-time symmetry, Proc. Natl. Acad. Sci. **119**, e2207543119 (2022).

[20] H. Xu, D. Mason, L. Jiang, and J. G. E. Harris, Topological energy transfer in an optomechanical system with exceptional points, Nature **537**, 80 (2016).

[21] K. Y. Fong, H.-K. Li, R. Zhao, S. Yang, Y. Wang, and X. Zhang, Phonon heat transfer across a vacuum through quantum fluctuations, Nature **576**, 243 (2019).

[22] J. Sheng, C. Yang, and H. Wu, Realization of a coupled-mode heat engine with cavity-mediated nanoresonators, Sci. Adv. **7**, eabl7740 (2021).

[23] M. J. Woolley and A. A. Clerk, Two-mode squeezed states in cavity optomechanics via engineering of a single reservoir, Phys. Rev. A **89**, 063805 (2014).

[24] Y. S. Patil, S. Chakram, L. Chang, and M. Vengalattore, Thermomechanical Two-Mode Squeezing in an Ultrahigh-Q Membrane Resonator, Phys. Rev. Lett. **115**, 017202 (2015).

[25] A. Pontin, M. Bonaldi, A. Borrielli, L. Marconi, F. Marino, G. Pandraud, G. A. Prodi, P. M. Sarro, E. Serra, and F. Marin, Dynamical Two-Mode Squeezing of Thermal Fluctuations in a Cavity Optomechanical System, Phys. Rev. Lett. **116**, 103601 (2016).

[26] W. H. P. Nielsen, Y. Tsaturyan, C. B. Møller, E. S. Polzik, and A. Schliesser, Multimode optomechanical system in the quantum regime, PNAS **114**, 62 (2017).

[27] T. Caniard, P. Verlot, T. Briant, P.-F. Cohadon, and A. Heidmann, Observation of Back-Action Noise Cancellation in Interferometric and Weak-Force Measurements, Phys. Rev. Lett. **99**, 110801 (2007).

[28] M. Tsang and C. M. Caves, Evading Quantum Mechanics: Engineering a Classical Subsystem within a Quantum Environment, Phys. Rev. X **2**, 031016 (2012).

[29] L. Mercier de Lépinay, C. F. Ockeloen-Korppi, M. J. Woolley, and M. A. Sillanpää, Quantummechanics-free subsystem with mechanical oscillators, Science **372**, 625 (2021).
[30] M. H. J. de Jong, J. Li, C. Gärtner, R. A. Norte, and S. Gröblacher, Coherent mechanical noise cancellation and cooperativity competition in optomechanical arrays, Optica **9**, 170 (2022).
[31] J. Wiersig, Enhancing the Sensitivity of Frequency and Energy Splitting Detection by Using Exceptional Points: Application to Microcavity Sensors for Single-Particle Detection, Phys. Rev. Lett. **112**, 203901 (2014).
[32] H.-K. Lau and A. A. Clerk, Fundamental limits and non-reciprocal approaches in non-Hermitian quantum sensing, Nat. Commun. **9**, 4320 (2018).
[33] J. P. Mathew, J. del Pino, and E. Verhagen, Synthetic gauge fields for phonon transport in a nano-optomechanical system, Nat. Nanotechnol. **15**, 198 (2020).
[34] J. del Pino, J. J. Slim, and E. Verhagen, Non-Hermitian chiral phononics through optomechanically induced squeezing, Nature **606**, 82 (2022).
[35] Y. S. S. Patil, J. Höller, P. A. Henry, C. Guria, Y. Zhang, L. Jiang, N. Kralj, N. Read, and J. G. E. Harris, Measuring the knot of non-Hermitian degeneracies and non-commuting braids, Nature **607**, 271 (2022).
[36] S. H. Nitzan, V. Zega, M. Li, C. H. Ahn, A. Corigliano, T. W. Kenny, and D. A. Horsley, Self-induced parametric amplification arising from nonlinear elastic coupling in a micromechanical resonating disk gyroscope, Sci. Rep. **5**, 9036 (2015).
[37] M. Defoort, P. Taheri-Tehrani, S. H. Nitzan, and D. A. Horsley, Impact of synchronization in micromechanical gyroscopes, J. Vib. Acoust. **139**, 040906 (2017).
[38] T. Antoni, K. Makles, R. Braive, T. Briant, P.-F. Cohadon, I. Sagnes, I. Robert-Philip, and A. Heidmann, Nonlinear mechanics with suspended nanomembranes, Eur. Phys. Lett. **100**, 68005 (2012).
[39] C. Samanta, P. R. Yasasvi Gangavarapu, and A. K. Naik, Nonlinear mode coupling an internal resonances in MoS_2 nanoelectromechanical system, Appl. Phys. Lett. **107**, 173110 (2015).
[40] D. Cadeddu, F. R. Braakman, G. Tütüncüoglu, F. Matteini, D. Rüffer, A. Fontcuberta i Morral, and M. Poggio, Time-resolved nonlinear coupling between orthogonal flexural modes of a pristine GaAs nanowire, Nano Lett. **16**, 926 (2016).
[41] D. Antonio, D. H. Zanette, and D. López, Frequency stabilization in nonlinear micromechanical resonators, Nat. Commun. **3**, 806 (2012).
[42] A. Eichler, M. del Álamo Ruiz, J. A. Plaza, and A. Bachtold, Strong Coupling between Mechanical Modes in a Nanotube Resonator, Phys. Rev. Lett. **109**, 025503 (2012).
[43] C. Chen, D. H. Zanette, D. A. Czaplewski, S. Shaw, and D. López, Direct observation of coherent energy transfer in nonlinear micromechanical resonators, Nat. Commun. **8**, 15523 (2017).
[44] A. Chandrashekar, P. Belardinelli, S. Lenci, U. Staufer, and F. Alijani, Mode Coupling in Dynamic Atomic Force Microscopy, Phys. Rev. Appl. **15**, 024013 (2021).
[45] P. M. Polunin, Y. Yang, M. I. Dykman, T. W. Kenny, and S. W. Shaw, Characterization of MEMS resonator nonlinearities using the ringdown response, J. Microelectromech. Syst. **25**, 297 (2016).
[46] J. Güttinger, A. Noury, P. Weber, A. M. Eriksson, C. Lagoin, J. Moser, C. Eichler, A. Wallraff, A. Isacsson, and A. Bachtold, Energy-dependent path of dissipation in nanomechanical resonators, Nat. Nanotechnol. **12**, 631 (2017).
[47] O. Shoshani, S. W. Shaw, and M. I. Dykman, Anomalous decay of nanomechanical modes going through nonlinear resonance, Sci. Rep. **7**, 18091 (2017).
[48] Y. Yan, X. Dong, L. Huang, K. Moskovtsev, and H. B. Chan, Energy Transfer into Period-Tripled States in Coupled Electromechanical Modes at Internal Resonance, Phys. Rev. X **12**, 031003 (2022).
[49] G. Anetsberger, R. Rivière, A. Schliesser, O. Arcizet, and T. J. Kippenberg, Ultralow-dissipation optomechanical resonators on a chip, Nat. Photonics **2**, 627 (2008).
[50] P. A. Truitt, J. B. Hertzberg, E. Altunkaya, and K. C. Schwab, Linear and nonlinear coupling between transverse modes of a nanomechanical resonator, J. Appl. Phys. **114**, 114307 (2013).
[51] M. H. J. de Jong, M. A. ten Wolde, A. Cupertino, S. Gröblacher, P. G. Steeneken, and R. A. Norte, Mechanical dissipation by substrate-mode coupling in SiN resonators, Appl. Phys. Lett. **121**, 032201 (2022).
[52] See Supplemental Material at http://link.aps.org/supplemental/10.1103/PhysRevApplied.20.024053 for derivations, detection-efficiency calibration, and coupling simulations. References [59–61] are cited in Supplemental Material.
[53] D. Høj, F. Wang, W. Gao, U. B. Hoff, O. Sigmund, and U. L. Andersen, Ultra-coherent nanomechanical resonators based on inverse design, Nat. Commun. **12**, 5766 (2021).
[54] R. Lifshitz and M. C. Cross, *Reviews of Nonlinear Dynamics and Complexity*, edited by H. G. Schuster (Wiley-VCH Verlag, Berlin, 2008).
[55] C. Samanta, N. Arora, and A. K. Naik, Tuning of geometric nonlinearity in ultrathin nanoelectromechanical systems, Appl. Phys. Lett. **113**, 113101 (2018).
[56] M. H. J. de Jong, A. Ganesan, A. Cupertino, S. Gröblacher, and R. A. Norte, Mechanical overtone frequency combs, Nat. Commun. **14**, 1458 (2023).
[57] A. Kanj, P. F. Ferrari, A. M. van der Zande, A. F. Vakakis, and S. Tawfick, Ultra-tuning of nonlinear drumhead MEMS resonators by electro-thermoelastic buckling, J. Acoust. Soc. Am. **152**, A38 (2022).
[58] L. E. Reichl, *A Modern Course in Statistical Physics* (John Wiley and Sons Inc., New York, 2016), 4th ed.
[59] P. Virtanen *et al.*, SciPy 1.0: Fundamental algorithms for scientific computing in Python, Nat. Methods **17**, 261 (2020).
[60] L. D. Landau and E. M. Lifshitz, *Mechanics* (Reed Educational and Professional Publishing Ltd., Linacre House, Jordan Hill, Oxford OX2 8DP, 1976), 3rd ed, Vol. 1.
[61] B. D. Hauer, C. Doolin, K. S. D. Beach, and J. P. Davis, A general procedure for thermomechanical calibration of nano/micro-mechanical resonators, Ann. Phys. (N. Y) **339**, 181 (2013).
[62] https://doi.org/10.4121/21428517.v1.